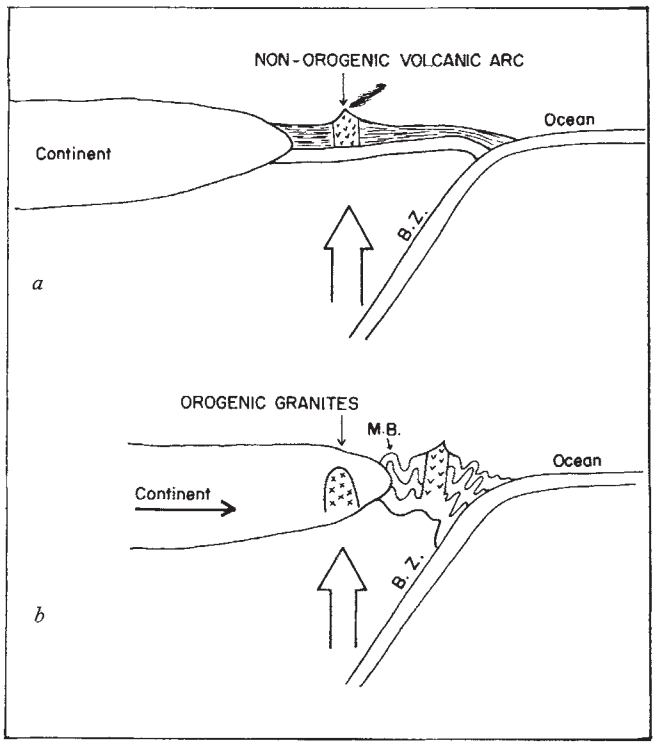

Fig. 5 Possible explanation for the relative positions of the non-orogenic volcanic arcs and orogenic granite belts. See text for discussion. BZ, Benioff zone; MB, median boundary of the paired metamorphic belts.

a paired metamorphic belt, the median boundary lying between the old landmass and the sedimentary belt.

The fossiliferous sedimentary belts probably all have a basement of oceanic crust which may be represented in at least one belt by an ophiolite complex[6]. Each new cycle represents the initiation of a new Benioff zone parallel to, but east of, the previous zone.

An important implication is that an ocean, like the Pacific, has existed to the east of New Zealand since at least the Cambrian. Japan shows a similar parallel development of paired metamorphic belts from the Palaeozoic to the present[14].

Relationship of volcanic arcs to metamorphic belts

The standard picture of a Pacific orogenic belt, as deduced, for example, from Japan[14], is that of a volcanic arc coinciding with the granitic metamorphic belt of high temperature/low pressure. In New Zealand, it seems that between orogenies the arc lay in the pre-orogenic sedimentary belt destined to suffer a high pressure metamorphism (Fig. 4); during the ensuing orogeny, the arc becomes transposed relatively to the west to lie under the old landmass. An explanation may be that an accelerated spreading rate during orogeny causes the landmass to compress and override the sedimentary rocks to the east, so that the high temperature effects are apparently transposed westwards (Fig. 5); in other words, it may be the continent that moves rather than the zone of high heat flow.

I thank M. G. Laird and J. D. Bradshaw for discussions.

Received September 22; accepted October 20, 1975.

1 Landis, C. A., and Coombs, D. S., *Tectonophysics*, **4**, 501–518 (1967).
2 Hatherton, T., *N.Z. Jl Geol. Geophys.*, **12**, 436–459 (1969).
3 Challis, G. A., *N.Z. Jl Geol. Geophys.*, **11**, 200–211 (1968).
4 Cooper, R. A., *N.Z. Jl Geol. Geophys.*, **18**, 1–20 (1975).
5 Force, E. R., *J. Geol.*, **82**, 37–49 (1974).
6 Blake, M. C., Jr, and Landis, C. A., *J. Res. U.S. Geol. Surv.*, **1**, 529–534 (1973).
7 Cooper, R. A., *N.Z. Jl Geol. Geophys.*, **17**, 955–962 (1974).
8 Adams, C. J. D., *Earth planet. Sci. Lett.* (in the press).
9 Bradshaw, J. D., and Andrews, P. B., *Nature phys. Sci.*, **241**, 14–16 (1973).
10 Blake, M. C., Jr, Jones, D. L., and Landis, C. A., in *The Geology of Continental Margins* (edit. by Burk, C. A., and Drake, C. L.), 853–872 (Springer, New York, 1974).
11 Grindley, G. W., *Geol. Map N.Z. (1:63,360), Sheet S8, Takaka* (DSIR, Wellington, New Zealand).
12 Gill, K. R., and Johnston, M. R., *N.Z. Jl Geol. Geophys.*, **13**, 477–494 (1970).
13 McDougall, I., and van der Lingen, G. J., *Earth planet. Sci. Lett.*, **21**, 117–126 (1974).
14 Miyashiro, A., *Metamorphism and Metamorphic Belts* (Allen and Unwin, London 1973).
15 Aronson, J. L., *Geochim. cosmochim. Acta*, **32**, 669–697 (1968).
16 Ghent, E. D., *Trans. R. Soc. N.Z. Geol.*, **5**, 193–213 (1968).
17 Wodzicki, A., *N.Z. Jl Geol. Geophys.*, **15**, 599–631 (1972).
18 Brown, W. H., Fyfe, W. S., and Turner, F. J., *J. Petrology*, **3**, 566–582 (1962).
19 Adams, C. J. D., Harper, C. T., and Laird, M. G., *N.Z. Jl Geol. Geophys.*, **18**, 39–48 (1975).
20 van Eysinga, F. W. B., *Geological Time Table*, 3rd Ed. (Elsevier, Amsterdam, 1975).
21 Laird, M. G., and Shelley, D., *N.Z. Jl Geol. Geophys.*, **17**, 839–854 (1974).
22 Shelley, D., *Jl R. Soc. N.Z.*, **5**, 65–75 (1975).
23 Brathwaite, R. L., *N.Z. Jl Geol. Geophys.*, **11**, 78–91 (1968).
24 Wodzicki, A., *N.Z. Jl Geol. Geophys.*, **17**, 747–757 (1974).

Summer phytoplankton blooms and red tides along tidal fronts in the approaches to the English Channel

R. D. Pingree & P. R. Pugh
Institute of Oceanographic Sciences, Wormley, UK

P. M. Holligan & G. R. Forster
Marine Biological Association of the United Kingdom, Plymouth, UK

Tidal mixing on the continental shelf in the South-western Approaches to the English Channel produces a situation in the summer where within a few miles the warmer surface water becomes completely mixed with the underlying colder water. These frontal boundaries may be followed for 100 nautical miles. By combining physical and biological oceanographic disciplines it has become clear that these boundaries are the sites of phytoplankton blooms which, in favourable conditions, may develop into red tides.

Our understanding of primary production in the sea seems to be hampered by an inadequate knowledge of the turbulent nature of the physical environment in which the phytoplankton exist. Progress in quantifying the distribution and growth rates of marine phytoplankton has taken two main directions; that of modelling[1–3], and the more statistical approach relating the variance and coherence of temperature and chlorophyll *a* to horizontal space scales[4–6]. Useful as the modelling approach has been in general, its main weakness is the uncertainty involved in specifying the mixing coefficients, which for the shelf region in the Western Approaches to the English

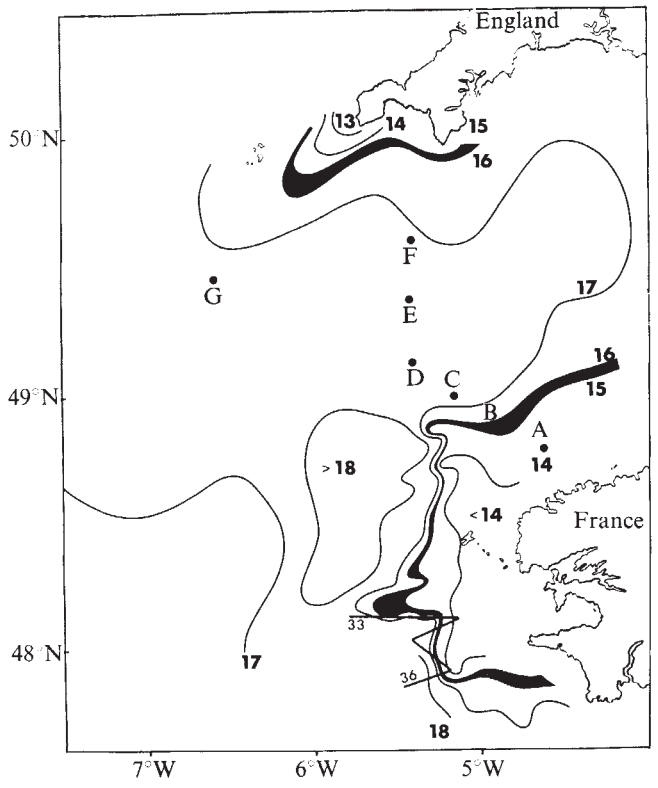

Fig. 1 Sea surface temperature contours obtained between July 26 and July 30, 1975. The 15–16 °C contours define the shelf front or the outcropping of the seasonal thermocline at the sea surface.

Channel may vary from 1 to 10^7 $cm^2\,s^{-1}$ (refs 7 and 8). The statistical approach is also a potentially valuable technique, but mechanisms of mixing which may be important in determining the distribution of phytoplankton are easily obscured. Here we show that the distribution and production rates of phytoplankton in the approaches to the English Channel are fundamentally linked with the turbulent nature of the environment. At this early stage a simple description of the possible operative mechanisms involved may be more illuminating and basic to our understanding than any attempt to define diffusion parameters or the statistical properties of the environment.

Surface temperature and chlorophyll *a*

It is surprising that for an area like the English Channel, where hydrographic data have been collected for nearly a century, and for which mean monthly temperature distributions were available in atlas form 40 yr ago[9], large surface temperature discontinuities that may be followed for up to 100 nautical miles (Fig. 1) have not been described. These structures mark the transition between well stratified shelf water and well mixed coastal water, or the outcropping of the thermocline at the sea surface. Stratification nearer the shore is also often evident, caused predominantly by warm, less saline water running off the land. Around the coast of France the transition can be defined by the maximum surface temperature gradient and in July 1975 was represented by the 15–16 °C surface temperature contours. In June 1974, it was similarly positioned and readily identifiable between the 13 and 14 °C contours[10]. With hindsight this feature can be recognised in earlier work[11], but it is, of course, more recent techniques, giving continuous records of hydrographic data, that have helped to define these regions clearly, and allow unambiguous interpretations that are often not possible with the more traditional methods based on sampling at discrete stations. Examples of continuous traces of temperature, salinity[12] and chlorophyll *a*[13] can be seen in Fig. 2. These traces were obtained south of Ushant (legs 33, 34 and 35, see Fig. 1) where the frontal characteristics were particularly well developed[14–16]. Here about 50%(~1.5 °C) of the temperature change across the region occurred within 3,000 m. Patches of floating weed were often evident in this zone[17] and also conspicuous was the frequent presence of fog over the cooler water. The lack of any large salinity changes (<0.03‰) or consistent correlations of salinity and temperature suggest that advection of warm surface water may not in general be responsible for the summer surface temperature distribution in the Western Approaches although historically the role of advection, rather than local surface heating and vertical mixing (over horizontal scales of the order of the tidal excursion), has been assumed dominant[18]. The chlorophyll *a* trace does, however, show a clear association with the temperature gradient. It is this association between temperature anomalies and phytoplankton distribution within the general framework of the presented hydrography, and the special circumstances that may bring about summer plankton blooms, and even red tides, which we are particularly concerned with here.

Vertical structures of temperature and chlorophyll *a* through a region of phytoplankton bloom

The vertical profiles of temperature and chlorophyll *a* were more conveniently investigated where the transition zone between well mixed and stratified regimes was broad, so that movement of the front itself during the measurements presented fewer difficulties. Indeed, on one station North-west of Ushant the water column appeared with a 3 °C temperature inversion, without a corresponding stabilising salinity change, reflecting frontal movement. The temperature and chlorophyll *a* data shown in Figs 3 and 4 can be placed geographically by reference to Fig. 1. Here the maximum surface temperature gradient between stratified and well mixed regimes occurs in the neighbourhood of station B. Station G has been included as representative of the extensive area of stratified water that is established on the shelf in the Western Approaches during the summer months. High values of chlorophyll *a* occur in surface waters in the frontal region. These extend well into the stratified side, and are also observed in the thermocline. The visual correlation with the temperature section is conspicuous. It would be misleading, however, to suggest that the phytoplankton distribution is controlled by temperature. The common factor producing these distribution patterns is water turbulence.

Fig. 2 Continuous surface temperature, salinity and chlorophyll *a* traces obtained south of Ushant (see Fig. 1, legs 33, 34 and 35). Note that the chlorophyll *a* trace responds with the temperature gradient (or perhaps more correctly near where the second differential of temperature with respect to time (distance) takes a positive sign).

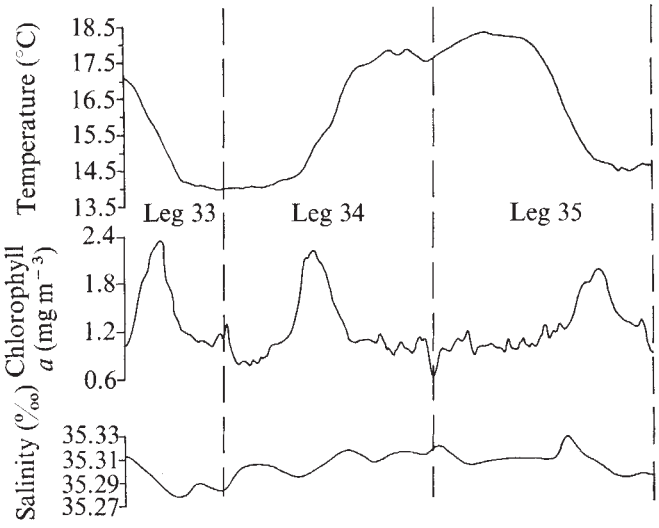

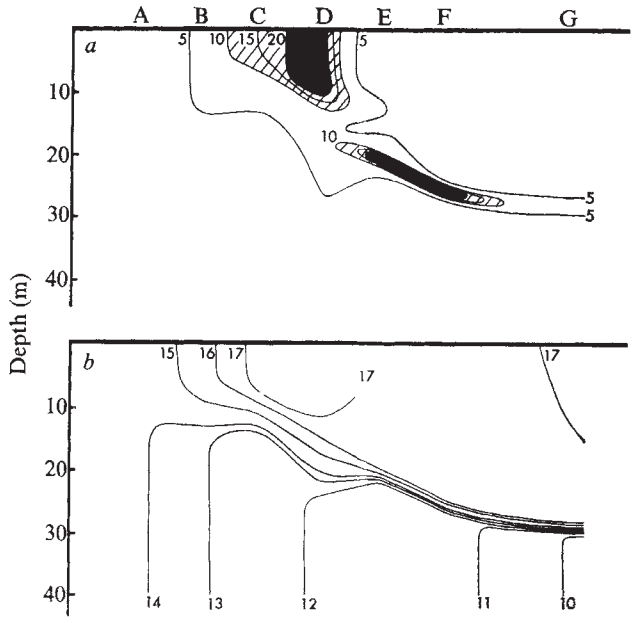

Fig. 3 *a*, Chlorophyll *a* section through the frontal region. The units of chlorophyll *a* concentration are mg m^{-3}. *b*, The corresponding temperature section. The units are in °C. Station positions A, B, C, D, E, F, G are as shown in Fig. 1.

In the stratified region three different mixing regimes can be identified, namely, the top mixed layer, the thermocline and the bottom mixed layer. The turbulence in the top mixed layer is derived from wind stress and night-time convection. The turbulent kinetic energy production has its maximum input near the surface. In the bottom mixed layer the turbulent energy is derived mainly from the tides, but near the shore, swell motion may also make a signficant contribution. In this region the turbulence declines away from the sea floor. The thermocline forms between the two mixed layers when the wind above the tide below can no longer stir the excess surface heating downwards. Here the ratio of the buoyancy flux to the turbulent energy production rate (that is, the local flux Richardson number) will be a maximum and the water column tends to stabilise, further inhibiting mixing. Towards the coast of France the tidal stream amplitude increases (Table 1) and the increased production rate of turbulent kinetic energy from below reduces the depth at which the thermocline can develop. The temperature section of Fig. 3 therefore represents the gradual change from the complete overlap which excludes the development of the thermocline to the situation where the wind and bottom mixed regimes are well separated vertically.

In general, differences in salinity will also contribute to the stability of the thermocline. The relative importance of salinity and temperature to the buoyancy flux can be determined from the ratio $\beta\Delta S/\alpha\Delta T$ where α is the coefficient of thermal expansion, β the coefficient of saline contraction and ΔT and ΔS are the corresponding temperature and salinity differences across the thermocline. This ratio was generally less than 5% (see Table 1) and so low that the temperature structure (Fig. 4) can also be considered as representative of the density structure.

In the stratified region, plant production in the surface layer is restricted by low levels of inorganic nutrients (Table 1, stations E, F, G). Values of chlorophyll *a* are also low below the thermocline, in spite of higher nutrient levels, because the mean light level is much reduced (generally less than 1% of the surface values). Why then are the values in the intermediate region in the thermocline as much as forty times larger than those above or below? Usual interpretations are based on phytoplankton aggregations due to sinking and settling on density discontinuities[19], or active downward swimming of flagellates towards the source of nutrients[20]. By considering a time scale for mixing, it can be illustrated that the interaction of the turbulence level with the levels of light and nutrients may largely determine the distribution characteristics of the chlorophyll *a* profiles.

Dispersal of phytoplankton in well mixed and stratified regions

Estimates for the lifetime of small scale structures in the sea have led to some interesting speculations concerning their generation and dissipation[21,22]. In a similar manner it is useful to have a diffusive time scale for the chlorophyll *a* structures in the water column. A characteristic time for a layer to mix above and below with its surroundings depends on the layer thickness, H, and the diffusion coefficient K. A time for mixing, t, may be defined by

$$t \sim H^2/4K$$

by analogy with the classical problem in heat flow, where t then represents the time taken for a uniformly heated layer to lose half its excess heat into a medium with the same conductivity[23].

In the bottom mixed layer the dominant stirring action of the tides produces a homogeneous temperature region in which the temperature gradient approaches the adiabatic value[24]. If close to the bottom, the diffusion coefficient may be written as[25]

$$K = 0.4u_*H$$

where the friction velocity u_* is defined from the bottom stress, τ_B, by $\tau_B = \rho u_*^2$, ρ is the density of seawater and H is the

Fig. 4 Vertical profiles of chlorophyll *a* and temperature obtained in: *a*, the well mixed (A); *b*, frontal (C); and *c*, stratified regions (E). The values are the original uncalibrated data which may be fixed absolutely by reference to Fig. 3.

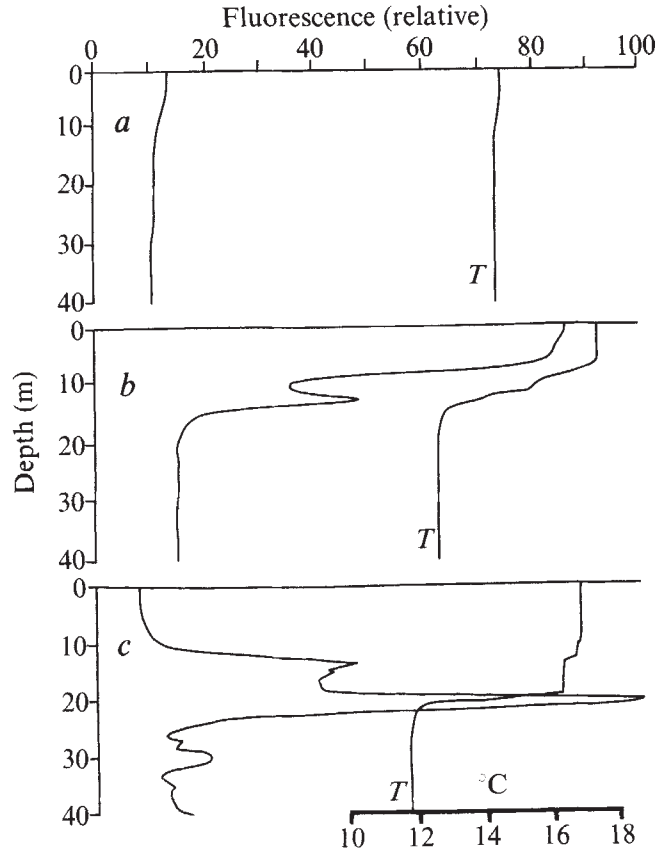

Table 1

Stations	A	B	C	D	E	F	G
Water depth (m)	92	98	107	108	106	94	110
Tidal stream amplitude at springs (m s^{-1})	1.3	1.1	0.9	0.8	0.7	0.7	0.6
Surface minus bottom temperature (°C)	0.2	2.7	5.1	5.7	5.3	5.4	7.5
Surface minus bottom salinity (‰)	0.01	0.024	0.065	0.060	0.043	0.067	0.074
Buoyancy flux ratio ($\beta\Delta S/\alpha\Delta T$) (%)		4	5	4	3	5	3
PO_4—P Surface layer 2 m	0.41	0.37	0.43	0.49	0.28	0.16	0.18
(μg atom l^{-1}) Bottom layer 40 m		0.39	0.39	0.42	0.50	0.61	0.73
NO_3—N Surface layer 2 m		2.56	1.79		0.1	0.69	0.25
(μg atom l^{-1}) Bottom layer 40 m		0.58	1.39		3.2	0.85	1.39
SiO_3—Si Surface layer 2 m	0.95	0.89	1.26		0.56	0.26	0.59
(μg atom l^{-1}) Bottom layer 40 m		0.85	0.74		0.63	0.93	1.23

height above bottom, then a mixing time scale for the bottom region of height H is

$$t \sim H/u_*$$

Here the validity of this relationship away from the bottom has been extended for illustrative purposes for an order of magnitude estimate. The bottom stress was determined from current meters placed 1, 2 and 3 m off the bottom at position 49°27′N, 4°42′W over a period of a month where the tidal streams were similar in amplitude to those in the neighbourhood of stations D and E. The semi-major axis of the semi-diurnal lunar, M_2, friction velocity was ~ 2 cm s^{-1} (ref. 26). This gives a time scale for mixing in this region below the thermocline of the order of 1 h during maximum tidal streaming. This is small in comparison with the division rate of phytoplankton cells[27] and does not permit a chlorophyll-rich zone to become established below the thermocline where the light intensity is still favourable. Furthermore the efficiency of mixing in this region explains why the small scale structures in the chlorophyll *a* profiles in the region below the thermocline (Fig. 4*c*) are transitory and not generally reproducible from profile to profile. The mixing efficiency in the bottom layer makes hypotheses concerning the migration of plant cells into nutrient-rich water less attractive since these cells risk being rapidly dispersed in the same manner as heat. Similar calculations can be made for a time scale in the wind-mixed layer, but as conditions at the sea surface are unpredictable the derived mixing values are less meaningful.

A time scale for the thermocline can be formed from

$$t \sim \frac{H^2\delta T/\delta z}{4F_h}$$

where F_h is the heat flux penetrating a thickness H of the thermocline of temperature gradient $\delta T/\delta z$

or

$$t \sim \frac{H(\theta_2-\theta_1)}{4F_h}$$

where $\theta_2-\theta_1$ is the temperature difference across the region H. Substituting typical values, $H = 5$ m, $\theta_2-\theta_1 = 4$ °C and $F_h = 2$ kcalorie cm^{-2} $month^{-1}$ (based on the warming rate of the bottom mixed layers), gives a time scale t, of about a week. This is large compared with the cell division rate of most phytoplankton. Thus, higher cell concentrations in the thermocline may simply reflect the reduced tendency for their dispersal by turbulence. The large time scale in the thermocline is consistent with the persistence of the chlorophyll *a* maximum in the thermocline from station to station. Cells in this region would also be first in line for nutrients brought up from below in the same manner that heat is continually mixed downwards.

In the well mixed region (Fig. 4*a*) there are both adequate light and nutrients (Table 1) for cell growth at the surface. The thoroughness of the mixing (or the short time scale), however, does not give the plant cells sufficient time in the surface layers to produce any marked degree of surface phytoplankton

Fig. 5 Aerial photograph from 6,000 feet (August 7, 1975; 1400 GMT) showing red tide effects in the neighbourhood of station C. Surface wind light and variable; sea state—low swell.

concentrations here. In a similar manner, vertical structures in both chlorophyll *a* and temperature profiles are conspicuously absent in this region.

Conditions favouring summer plankton blooms

The frontal region represents an area of recently stabilised mixed water in which the combination of high nutrients and a shallow upper mixed layer create conditions suitable for the rapid growth of phytoplankton[28]. These conditions are particularly dependent on weather and tide. At spring tides, for example, the tidal stream amplitude is approximately double that at neap tides, with a corresponding cubed production rate of turbulent kinetic energy in the bottom mixed layer, causing the well mixed region to increase in size at the expense of the more stratified region and nutrients to be brought to the surface. As the tidal streams slacken towards neaps, the surface water stabilises and conditions are set for a plankton bloom. In a similar manner, a period of turbulent weather will cause the frontal boundary to move into the stratified region, particularly if this is also the wind direction. Indeed a continual series of blooms may be created by the interaction of weather and tide as the balance between stabilisation and increasing turbulence is altered along this shallow thermocline region. It is worth remarking that it is the shallowness of the thermocline in this region that largely determines the size of the area likely to be effectively mixed and subsequently to produce favourable growth conditions. Our observations were made during calm weather following a period of spring tides and strong winds, which perhaps accounts for the large size of the region in bloom condition. The high surface values for dissolved inorganic nutrients at stations C and D, which exceeded those at 40 m (Table 1), cannot yet be explained.

Red tide characteristics within bloom region

Although so far we have not found it necessary to consider the swimming activities and buoyancy effects of the phytoplankton cells it is evident that they must be important on smaller scales within the bloom region. Dominant in the frontal region was the dinoflagellate *Gyrodinium aureolum* Hulburt, a species that has been reported as occurring in high concentrations in other areas[29–31]. Counts of a representative sample (34 mg chlorophyll *a* per m^3) gave the following values (cells per 1×10^6): *G. aureolum*, 1.7; *Prorocentrum micans* Ehr., 0.01; flagellates, 1.4; and all other photosynthetic cells, 0.005. Areas were found where the concentration of chlorophyll *a* was as high as 100 mg m^{-3}. A week later these reddish-brown streaks were observed from a height of 6,000 feet (Fig. 5), which were aligned in parallel but broken and irregular rows typical of a red-tide phenomenon[32]. A conservative estimate[33–35] would suggest these patches contain more nutrients than were available in the water, and it seems unlikely that they could be produced without any interaction between cell movement and water turbulence. Concentrating mechanisms might be based on a daytime upward migration[43] coupled with weakly organised Langmuir circulations[36], or on the interaction between phytoplankton movement and internal waves[37]. Red tide effects have also been reported from inshore regions, though these are often due to positively buoyant organisms such as *Noctiluca*[38,39].

Primary production in characteristic regions

Interesting as these distributions of phytoplankton standing crop are, they are not a measure of primary production in the various regions. Rates of carbon dioxide fixation were determined by inoculating appropriate water samples with $NaH^{14}CO_3$ and incubating them at sea surface temperature under fluorescent lights in the ship's laboratory or *in situ* under natural light at various depths. The data are summarised in Table 2. Mean values for chlorophyll *a* are representative for the vertically mixed regime in the neighbourhood of station A, for the frontal region between stations B and D, and for the top and bottom mixed layers in the stratified region. The thermocline is considered to be between 25 m and 30 m, and a mean value for chlorophyll *a* across the most concentrated 5 m of the chlorophyll peak is given. The assimilation index (AI)[27] is the potential for carbon fixation under light saturation (equivalent to 10% midday summer sunlight)[40]. High indices were found for plant populations in the thermocline and in the vertically mixed regime. Lower indices for other regions may reflect a lack of dissolved nutrients or a poor physiological condition of the cells. In the frontal region the assimilation index seems to be inversely related to cell concentration, and for a higher chlorophyll *a* concentration of 78 mg m^{-3} a value of 1.34 mg carbon per h per mg chlorophyll *a* was observed.

Rates of primary production *P* were calculated from the equation

$$P = \text{AI chlorophyll } a \int_0^z I_0 e^{-kz} dz$$

(where I_0 is subsurface light intensity and *z* is depth of the water column) and expressed relative to a value of unity for the vertically mixed regime. In the stratified regime, for which the relative production rate is greater than one, the phytoplankton in the thermocline account for at least 50% of the total carbon fixation. Some caution is necessary in specifying this proportion since it will vary with light intensity. For example, under high surface light intensities photosynthesis will be maximal in the thermocline but saturated or light-inhibited in the top mixed layer. The production occurring below the thermocline seems relatively unimportant. In the frontal region, in spite of both the high extinction coefficient and the low assimilation index, the relative production is high. Thus, it seems that this weakly stratified region has an important bearing on primary production in the English Channel in the summer, and, furthermore, it is notable that the turbulent structure is also important in determining the rate of production of phytoplankton as well as the distribution pattern for the standing crop.

It is clear that further studies on primary production and the distribution of chlorophyll *a* in other associated frontal systems in the English Channel, for example, around the Lizard and Land's End (see Fig. 1), are necessary. Further work also needs to be directed towards answering questions such as which of

Table 2 Primary production data

	Mixed	Frontal	Stratified		
			Wind mixed layer	Thermocline	Bottom mixed layer
Chlorophyll *a* (mg m^{-3})	0.45	19.0	0.55	9.5	0.66
Extinction coefficient *k* (m^{-1})	0.12	0.34	0.10	$0.1 < k < 0.3$	0.10
Assimilation index (AI) (mg C fixed per h per mg chlorophyll *a*)	4.2	1.9	2.2	5.7	0.2
Relative production rate (*P*)	1.0	6.5	0.6	0.7–1.1 1.6	0.05

the three regions, well mixed, frontal or stratified, is generally the most productive; what are the relative contributions of the top mixed layer, thermocline and bottom mixed layer to the total production of the water column in the stratified regime; and how representative is a single station, like E1 (ref. 41), of production in the English Channel? The interrelationship between the distribution of phytoplankton and herbivorous zooplankton is poorly understood, particularly for the stratified regime. It seems probable that the high concentration of plant cells in the thermocline is an important food source for both migratory[42] and non-migratory grazing organisms.

We thank Captain Dowell and the officers and crew of RV Sarsia for assistance at sea.

Received October 7; accepted November 18, 1975.

1 Steele, J. H., *Nature*, **248**, 83 (1974).
2 Platt, T., and Denman, K. L., *Mém. Soc. r. Sci. Liège*, **7**, 31 (1975).
3 O'Brien, J. J., and Wroblewski, J. S., *J. Theor. Biol.*, **38**, 197–202 (1973).
4 Platt, T., *Deep Sea Res.*, **19**, 183–188 (1972).
5 Denman, K. L., and Platt, T., *Mém. Soc. r. Sci. Liège*, **7**, 19 (1975).
6 Fasham, M. J. R., and Pugh, P. R., *Deep Sea Res.* (in the press).
7 Pingree, R. D., and Pennycuick, L., *J. mar. biol. Ass. U.K.*, **55**, 261–264 (1975).
8 Pingree, R. D., Pennycuick, L., and Battin, G., *J. mar. biol. Ass. U.K.*, **56**, 975–992 (1975).
9 Lumby, J. R., *Fishery Invest. Ser.* 2, **14**, 1–67 (1935).
10 Pingree, R. D., *J. mar. biol. Ass. U.K.*, **56**, 965-974 (1975).
11 Matthews, D. J., *Rep. N. Sea Fish. Invest. Comm. 3, 1906–08*, 269–282 (1911).
12 Pingree, R. D., *Deep Sea Res.*, **16**, 275–295 (1969).
13 Lorenzen, C. J., *Deep Sea Res.*, **13**, 223–227 (1966).
14 Grall, J. R., Fèvre-Lehoerff, G., and Fèvre, J. Le, *Cah. océanogr.*, **23**, 145–170 (1971).
15 Fearnhead, P. G., *Deep Sea Res.*, **22**, 311–321 (1975).
16 Simpson, J. H., and Hunter, J. R., *Nature*, **250**, 404–406 (1974).
17 Pingree, R. D., Forster, G. R., and Morrison, G. K., *J. mar. biol. Ass. U.K.*, **54**, 469–479 (1974).
18 Cooper, L. H. N., *J. mar. biol. Ass. U.K.*, **39**, 637–658 (1960).
19 Smayda, T. J., *A. Rev. Oceanography mar. Biol.*, **8**, 353–414 (1970).
20 Eppley, R. W., Holm-Hansen, O., and Strickland, J. D. H., *J. Phycol.*, **4**, 333–340 (1968).
21 Stommel, H., and Fedorov, K. N., *Tellus*, **19**, 306–325 (1967).
22 Tait, R. I., and Howe, M. R., *Deep Sea Res.*, **15**, 275–280 (1968).
23 Prandtl, L., *The Essentials of Fluid Dynamics* (Blackie, London and Glasgow, 1952).
24 Pingree, R. D., and Griffiths, D. K., *Nature*, **250**, 720–722 (1974).
25 Carslaw, H. S., and Jaeger, J. C., *Conduction of Heat in Solids* (Oxford University Press, Oxford, 1959).
26 Channon, R. D., and Hamilton, D., *Nature*, **231**, 383–385 (1971).
27 Eppley, R. W., *Fish. Bull. natn. oceanic atmos. Adm. U.S.*, **70**, 1063–1085 (1972).
28 Wyatt, T., and Horwood, J., *Nature*, **244**, 238–240 (1973).
29 Braarud, T., and Heimdal, B. R., *Nytt. Mag. Bot.*, **17**, 91–97 (1970).
30 Hickel, W., Hagmeier, E., and Drebes, G., *Helgolander Wiss. Meeresunters*, **22** 401–416 (1971).
31 Ballantine, D., and Smith, F. M., *Br. phycol. J.*, **8**, 233–238 (1973).
32 Parsons, T. R., Stephens, K., and Strickland, J. D. H., *J. Fish. Res. Bd Can.*, **18**, 1001–1016 (1961).
33 Holmes, R. W., Williams, P. M., and Eppley, R. W., *Limnol. Oceanogr.*, **12**, 503–512 (1967).
34 Loftus, M. E., and Seliger, H. H., *Chesapeake Sci.*, **16**, 79–92 (1975).
35 Bainbridge, R., *Biol. Rev.*, **32**, 91–115 (1957).
36 Langmuir, I., *Science*, **87**, 119–123 (1938).
37 Kamykowski, D., *J. mar. Res.*, **32**, 67–89 (1974).
38 Fèvre, J. Le, and Grall, J. R., *J. exp. mar. Biol. Ecol.*, **4**, 287–306 (1970).
39 Wilson, D. P., *Life of the Shore and Shallow Sea* (Nicholson and Watson, London 1935).
40 Ryther, J. H., *Limnol. Oceanogr.*, **1**, 61–70 (1956).
41 Russell, F. S., Southward, A. J., Boalch, G. T., and Butler, E. I., *Nature*, **234**, 468–470 (1971).
42 Southward, A. J., *J. mar. biol. Ass. U.K.*, **42**, 275–375 (1962).
43 Eppley, R. W., and Harrison, W. G., *AEC Progress Rep. Research on Marine food Chain*, 208–221 (1975).

Models for metal ion function in carbonic anhydrase

Paul Woolley

Max-Planck Institute for Biophysical Chemistry, 34 Göttingen-Nikolausberg, West Germany

A model catalyst is described which has properties in common with carbonic anhydrase. The model demonstrates the availability of a mechanism, previously only hypothetical, for the action of the enzyme. It also shows, however, that this mechanism alone is not adequate to produce the high activity of the enzyme.

DETECTED in 1928, discovered in 1932, recognised to contain zinc in 1939, obtained pure in 1959, crystallised in 1962 and the subject of some 1,800 papers and articles, carbonic anhydrase continues to elude a full mechanistic description, even though this enzyme is small, stable and easily isolated, and its X-ray structure is known to a resolution[1,2] of 2 Å.

Carbonic anhydrase catalyses a range of reactions, including the hydration of carbon dioxide and aldehydes, and the hydrolysis of carboxylic, sulphonic and carbonic esters. The CO_2 hydration is apparently the reaction of biological importance, both in respiration and in intracellular CO_2–HCO_3^- equilibration. In most of these reactions the rate in the absence of enzyme is believed to be limited by the nucleophilic attack of an oxygen atom or ion at an electrophilic centre, usually carbon, illustrated in Fig. 1*a*. The enzyme accelerates the CO_2 hydration, the acetaldehyde hydration and the hydrolysis of *p*-nitrophenyl acetate by factors of 10^9, 10^5 and 10^5 respectively over the reaction in water.

The zinc ion which occurs naturally in carbonic anhydrase may be replaced artificially by other metal ions, but only cobalt(II) and zinc confer appreciable activity on the enzyme; with no metal or with other metals the enzyme is practically inactive in hydration.

The enzyme possesses an ionising group with a pK_a of about 7; only the alkaline form of the enzyme is catalytically active.

One elegant mechanistic suggestion[3] is that a metal-bound water molecule could ionise to provide the necessary nucleophile in the form of metal-bound hydroxide (Fig. 1*b*). Other possibilities include the ionisation of a nearby histidine group to provide a general-base catalyst at the active site[4]; the zinc could then act as a point of substrate binding, perhaps also polarising and thereby activating the substrate by virtue of its Lewis acid strength[5]. Whatever the mechanism of nucleophilic attack, other stages of the reaction may also be catalysed, such as proton transfer within the enzyme–substrate complex[6] or between the enzyme and its aqueous environment[7].

The purpose of this article is to re-examine the plausibility of the first mechanism referred to above, the zinc-bound hydroxide nucleophile (ZHN) hypothesis. Reviews and background literature are given in refs 2 and 8.

A priori arguments against the ZHN mechanism have been twofold: first, that a zinc-bound water cannot have such a low pK_a as 7 (refs 4 and 9); second, that a zinc-bound hydroxide ion would be so polarised by the zinc as to lose most of its negative charge to the zinc and thus be too weak a nucleophile to attack, for example CO_2 (refs 6 and 10 and Fig. 1*b*). Transition-metal hydroxy complexes can indeed attack CO_2 (refs 11 and 12), but so far few quantitative data are available.

To investigate the universality of these two presuppositions, model systems were chosen to reflect closely the desired properties of the enzyme. The much-abused term "model" is here understood as a simple chemical system with a property or properties relating it to the biological system under consideration. Ideally a range of model compounds, structurally controlled to reproduce in varying degrees the property in question, provide a quantitative scale on which the biological system